Effect Of Ar^{2+} Ion Irradiation On Microstructure And Mechanical Properties Of Chromium-Coated Zirconium Alloy At 400°C

Wang Xinyi [1,], Tang Dewen[1,2*], Liu Yunjie[1]

[1] School of mechanical engineering, University of South China, Hunan, Hengyang, 421001
[2] Hunan Provincial Key Laboratory of Emergency Safety Technology and Equipment for Nuclear Facilities, University of South China, Hunan, Hengyang, 421001

Abstract: Following the Fukushima incident, there has been a surg e in research and development of chromium (Cr) coatings for zirco nium (Zr) alloy cladding. The majority of these studies have conce ntrated on the high-temperature oxidation resistance of these coatin gs, with less emphasis on their high-temperature irradiation resistan ce. To address this gap, an integrated approach combining argon io n irradiation experiments with computational simulations was emplo yed to assess the influence of varying ion irradiation dose on the microstructural and mechanicalattributes of chromium-coated zirconi um alloy under irradiation at 400℃. The post-irradiation microstruc ture, phase composition, and mechanical properties of the chromiu m coated zirconium alloy were examined using a suite of analytica l techniques, including scanning electron microscope, transmission e lectron microscope,energy-dispersive X-ray spectroscopy, tensile testi ng, and X-ray diffraction. The findings reveal that the extent of irr adiation-induced damage correlates positively with the Ar ion irradi ation dose, and that higher doses of irradiation promote the progres sive development of a dense dislocation network, thereby significan tly enhancing the coating's hardness. This observation underscores t he commendable resistance to corrosion of chromium coatings.

Keywords: Chromium coating; Zirconium alloy; Ion-irradiation; Irradiation hardening.

1.Introduction

Since the Fukushima nuclear accident, the notion of accident-tolerant fuel (ATF) has gained prominence. Coated zirconium alloy cladding, which shows numerous advantages and broad potential applications, has been identified as the near term solution for ATF in many countries. This cladding is primarily derived from commercially available zirconium alloy cladding, with the addition of a superior antioxidant coating on the outer surface. Over the past decade, a variety of cladding materials for Zr alloys have been proposed1, including silicon carbide, iron-chromium-aluminium alloys and chromium coatings 5-6. Among the various contenders, chromium coatings have been widely used due to their relatively low thermal neutron absorption cross section of 2.9 barns, a coefficient of thermal expansion closely matching that of Zr alloys (with a difference of approximately 0.9×10^{-6} K^{-1}), and

* Corresponding author : will998@163.com

their outstanding resistance to corrosion and oxidation 78. However, in terms of actual in-reactor conditions, cladding materials are typically subjected to prolonged exposure and high levels of irradiation prior to reaching an accident state. Zirconium alloy cladding materials are susceptible to creep fatigue and thermal shock within reactors, and their coatings are at risk of delamination due to the significant disparity in properties between the coating and the substrate during stress, oxidation, and other factors. This can lead to a loss of protective capabilities for the substrate.

While numerous domestic research institutes have also conducted research on accident-resistant fault-tolerant fuel technology, as referenced in literature [9-12]. However, their researches have predominantly centered on the coating preparation process and the ex-reactor performance of chromium coatings, with a notable absence of research on the neutron irradiation behavior of these materials. Investigations into the neutron irradiation behaviour of nuclear materials are still constrained by the high cost and extended durations associated with irradiation testing. Extensive researches have demonstrated that ion irradiation can effectively replicate the key microstructural characteristics observed in materials irradiated with neutrons. Ion irradiation offers numerous benefits, including the ability to achieve high levels of displacement damage, the flexibility to adjust irradiation parameters, and the generation of low induced radioactivity. Consequently, ion irradiation has become a prevalent method for simulating radiation damage in structural materials used within nuclear reactors 13.

Elevated irradiation doses result in increased dislocation loop density within crystalline structures that can cause multiplication of dislocation loops. As a result, both the irradiation dose and temperature are pivotal parameters influencing the dislocation loop density and the post-irradiation microstructural characteristics of a material. Jiang et al.14 have reported that Au^{+} irradiation at 400°C produces a higher dislocation loop density, with the evolution of irradiation-induced defects being retarded in thinner chromium coatings. Li et al.15 employed molecular dynamics simulations to investigate the evolution of structural defects at the coating interface under energetic particles irradiation. They analysed the impact of irradiation dose on the coating damage and proposed the enhancement of coating interface density as a strategy to mitigate irradiation damage. Extensive domestic and foreign research groups have conducted studies on irradiation damage on chromium coatings, observing immediate swelling post-ion irradiation and the formation of voids at doses of 1-2 displacements per atom (dpa) **Error! Reference source not found.Error! Reference source not found.**. Notably, both the size and density of dislocation loop escalate with the increase of irradiation dose, especially at higher irradiation dose.

This study employs a synergistic approach of simulation and experimental testing to assess the performance of argon (Ar) ion irradiation on chromium-coated zirconium alloys. The primary objective is to elucidate the influence of irradiation dose on the microstructural and mechanical properties of the alloys at 400°C. Comparative morphological analyses of both unirradiated and irradiated samples were conducted at the specified irradiation temperature using scanning electron microscopy (SEM). Additionally, the composition and phases of the samples were examined using energy-dispersive spectroscopy (EDS) and X-ray diffraction (XRD). Hardness tests were performed to ascertain the impact of irradiation dose on the coating's morphology, the composition of physical phases, and the irradiation-induced hardening. Finally, transmission electron microscopy (TEM) was utilized to acquire grain size and crystal structure of the samples, providing a comprehensive understanding of the irradiation effects.

2.Experimental details

2.1 Sample preparation

The experimental substrate consisted of Zr-4 alloy plates, which were wire-cut into block specimens measuring 15 mm × 15 mm × 2.2 mm. The specimens underwent a series of polishing steps using diamond abrasive papers with grits of 400#, 600#, 800#, 1200#, 1500#, and 2000#, followed by metallographic abrasive papers of 2500#. This polishing sequence was repeated to ensure a uniform and smooth surface finish. The specimens were then meticulously polished with 2500# metallographic sandpaper and finally brought to a mirror-like finish using a mechanical polishing machine and chromium oxide polishing powder (with particle sizes ≤ 0.1 μm). Post-polishing, the specimens were cleaned with deionized water, ultrasonically rinsed in anhydrous ethanol for 15 minutes, and subsequently air-dried.

2.2 Ion irradiation test

The ion irradiation experiments were conducted utilizing the 400 kV ion implanter in the triple-ion-beam combining facility designed by the Energy College of Xiamen University. For these experiments, Ar^{2+} ions at an energy level of 400 keV were selected as the irradiating species. The temperature during irradiation was maintained at 400°C, and the Ar^{2+} ion fluences were set at three distinct levels: 5×10^{16} ions/cm^2, 1×10^{17} ions/cm^2, and 2×10^{17} ions/cm^2.

Fig.1. Schematic diagram of ion implantation

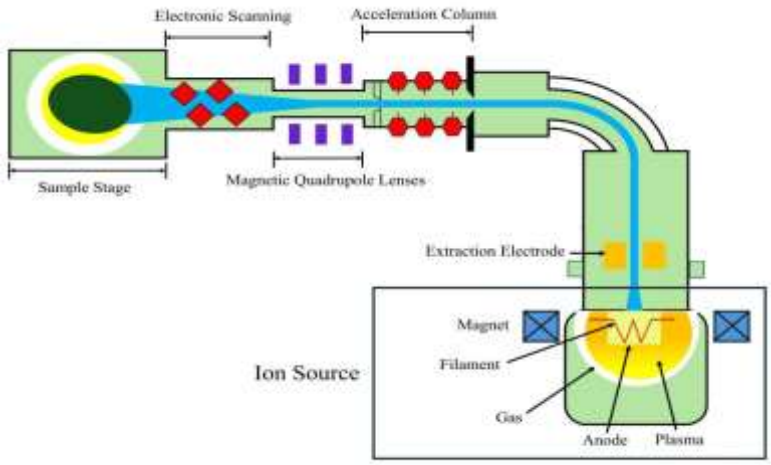

Ion irradiation induces inhomogeneous radiation damage at various depths within the material. To address this, the study of the coatings was designed to mitigate the influences of both the surface effects and the irradiated noble gas atoms. In order to ascertain the displacements per atom (dpa) and the region of injected Ar^{2+} atoms, the damage inflicted by these ions on the material was quantified using SRIM's Fast Damage Kinchin-Pease model 19. This software simulates the interactions between the incoming and outgoing Ar^{2+} and the target atoms, employing the Monte Carlo statistical method to calculate the stochastic collisions between recoil atoms and target atoms. Consequently, the valuation of each physical quantity can be obtained by simulating the motion process after the bombardment of the target by incoming and outgoing ions by SRIM software and performing the calculation. Equation (1) presents the formula for determining the number of Ar2+ ions and the extent of damage (dpa) incurred 12.

$$D_{dpa} = \frac{V\Phi \times 10^8}{\rho} \square \quad (1)$$

The formula employed to calculate the irradiation damage (dpa) takes into account the number of vacancies (V) generated within the specimen, as determined by the SRIM software, the irradiation dose (Φ) expressed as the number of ions per cubic centimeter, and the atomic number density (ρ) of the specimen, which is the number of atoms per cubic centimeter. For chromium (Cr), the atomic number density is specified as 8.338×10^{22} atoms/cm^3. The displacement energy and density of the chromium coating were set to 40 eV and 7.2 g/cm^3, respectively 2023. According to the simulation results, the maximum displacement damage produced by the irradiation of the chromium coating by Ar^{2+} ions at 400 keV is 47.4dpa.

Fig.2. SRIM prediction for damage production and implanted Ar^{2+} ions distributions for the chromium-coated zirconium alloy sample

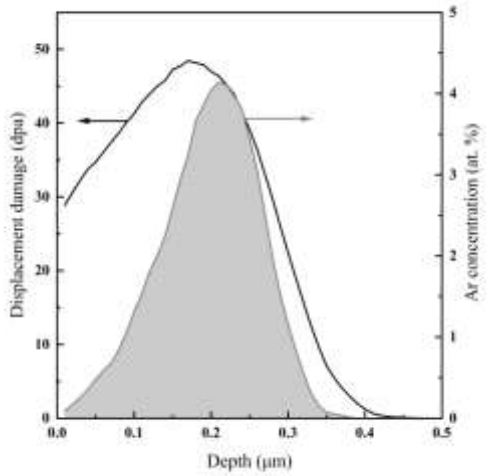

2.3 Coating characterization

The X-ray diffraction (XRD) analysis was conducted using a Smart lab SEM from Rigaku, Japan, which was operated at a grazing angle of 2° with a scanning range from 20° to 90° using a Cu target and a step size of θ = 0.02°. The samples were further characterized for irradiation damage and micro-morphological features using scanning electron microscopy (SEM) and energy-dispersive spectroscopy (EDS). The SEM analysis was performed by using a TESCAN CLARA series microscope, capable of analyzing the microstructural morphology of the materials in both secondary electron (SE) and backscattered electron (BSE) modes. For the observation of the cross-sectional morphology of the samples, a JEOL JEM-F200 transmission electron microscope was utilized. The samples were prepared by thinning with a TESCAN AMBER GMH focused ion beam (FIB). The elemental content of the materials was calibrated using an Oxford Instruments Xplore 30 series spectrometer.

2.4 Hardness test

A Vickers hardness tester, model HVS 1000AV, was utilized to assess the hardness of the chromium coatings. The hardness testing parameters are set with load of 200 g and dwell time of 5 seconds. To determine the hardness, an average of ten measurements was taken at intervals of 5 mm across the

coating surface. This approach involved calculating both the mean and variance of the hardness values. The hardness data obtained from these measurements served as a basis for comparing the hardness of the coatings before and after irradiation. This comparison was crucial for understanding the influence of irradiation and the irradiation dose on the irradiation hardening effects within the chromium coatings.

3. Results and discussion

3.1 XRD and microscopic morphology

Figure 3 shows the XRD spectra of the specimens surface both prior to and following irradiation. The XRD patterns of all irradiated samples displayed two distinct diffraction peaks characteristic of body-centered cubic (BCC) chromium (Cr): corresponding to the Cr (110) plane at 44.4° and another at 64.6°corresponding to the Cr (200) plane. Notably, the (110) peak was more intense than the (200) peak, a feature that was consistent with the unirradiated samples. Upon increasing the ion fluence, the (200) peak shifted towards a higher angle, while the (110) peak shifted towards a lower angle. This shift indicates an increase in the (200) crystal plane spacing and a decrease in the (110) crystal plane spacing, respectively. According to Wan et al.24, such variations in crystal plane spacing are associated with the aggregation of interstitial atoms and the aggregation of vacancies. The analysis suggests that as the ion incident dose increases, the probability of cascading collisions rises, leading to the generation of more point defects within the material. These point defects, in turn, facilitate the formation of vacancy defect clusters, which results in an increase in the crystal spacing of the (200) plane.

Although irradiation did not alter the phase structure of the chromium coating, it did result in a broadening of the (110) peak post-irradiation. In addition, the irradiated (110) peak is positioned to the right of the standard position of Cr (110) peak, suggesting a reduction in the planar distance along the out-of-plane direction. The shift of the diffraction peak to a higher angle may imply the presence of tensile stresses. High melting point metal, such as chromium films, typically exhibit inherent tensile residual stresses, especially when the films have columnar pores 2527. As the irradiation dose increases, the (200) peak shifts further towards higher angles, and the (110) peak shifts towards lower angls, signifying increased lattice distortion. This distortion implies changes in interatomic distances and forces within the material.

Fig.3. XRD spectra of irradiated and unirradiated chromium-coated zirconium alloy sample surfaces

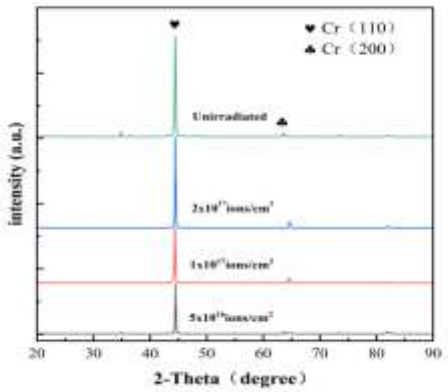

Figure 4 is the scanning electron microscopy (SEM) morphologies of the material surface before and after exposure to various doses of Ar^{2+} ion irradiation. The unirradiated chromium coating exhibits a rough and uneven surface texture, with isoperimetric crystal grains and significant gaps between them, along with a few surface holes. The presence of large particles on the surface of multi-arc ion plating chromium coatings is a typical feature of deposition technique. This phenomenon occurs due to the high cathodic arc spot temperature, which leads to uneven ablation. Under the bombardment of high-energy particles, molten metal droplets splash and deposit on the substrate, solidifying as particles 2829. The large particles produce a shadowing effect on the coatings, contributing to the generation of pores on the surface of the multi-arc ion plating coating 30. Atomic sputtering is identified as the primary cause of surface defects formation in alloys. Upon irradiation, the large particles on the surface of the irradiated chromium coating undergo significant changes. This is attributed to the higher energy of incident particles during the coating deposition process. The higher energy particles have a greater probability of migration, and transfer their kinetic energy to other particles on the coating surface, leading to re-sputtering phenomenon, which will be able to reduce the number of holes. After irradiation, the coating surface remains intact without flaking off. Furthermore, the surface coating does not blister under varying irradiation doses, demonstrating the coating's high resistance to irradiation-induced damage.

Fig.4. The surface morphology of the irradiated and unirradiated chromium-coated zirconium alloy sample

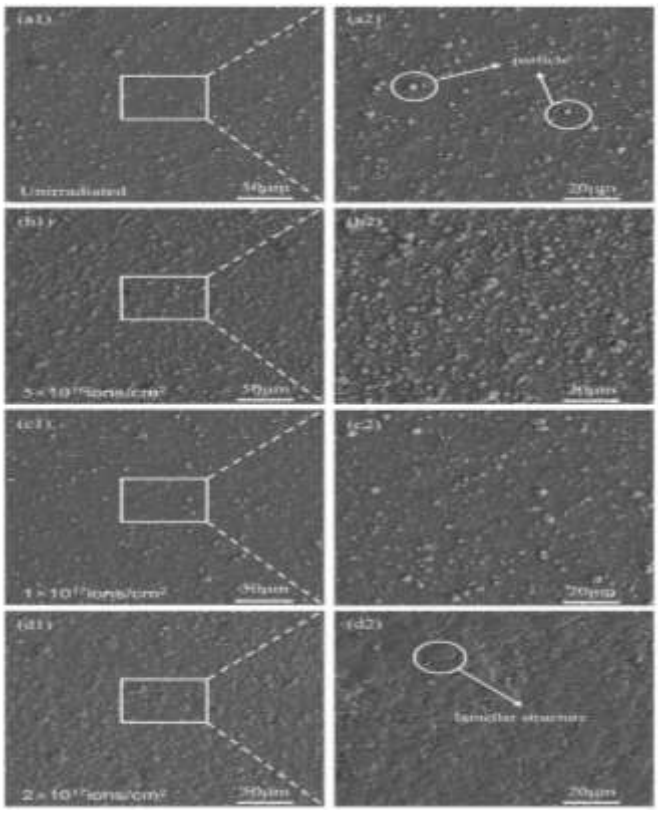

Figure 5 illustrates the scanning electron microscopy (SEM) morphologies of the coating's cross-section before and after exposure to different doses of Ar^{2+} ion irradiation. The formation of pores and bumps on the material surface can be attributed to the action of Ar^{2+} ions, which cause atoms to sputter from the solid surface, leading to localized exfoliation and the creation of holes. Concurrently, the sputtered atoms accumulate at other locations on the surface, forming bumps. After

irradiation, the coating fragments maintained an intact surface without any flaking off. The number and area of irradiation-induced defects within the chromium coating cross-section increases with both the irradiation dose and the depth of ion penetration. Irradiation accelerates diffusion processes within the specimen, with the structural defects induced by irradiation serving as diffusion channels for oxygen (O), zirconium (Zr), and chromium (Cr). Additionally, irradiation may induce amorphization of the zirconium matrix surface.

Examination of the unirradiated sample reveals that the chromium coating is composed of columnar crystals that are oriented perpendicularly to the interface with the substrate. Notably, the size of these columnar crystals increases progressively as they extend away from the coating-substrate interface. After irradiation, the original columnar crystal structure of the cross-sectional coating is observed to undergo partial alteration, with the destruction of the columnar crystals being a significant change.

Fig.5. The cross-section morphology of the irradiated and unirradiated chromium-coated zirconium alloy sample

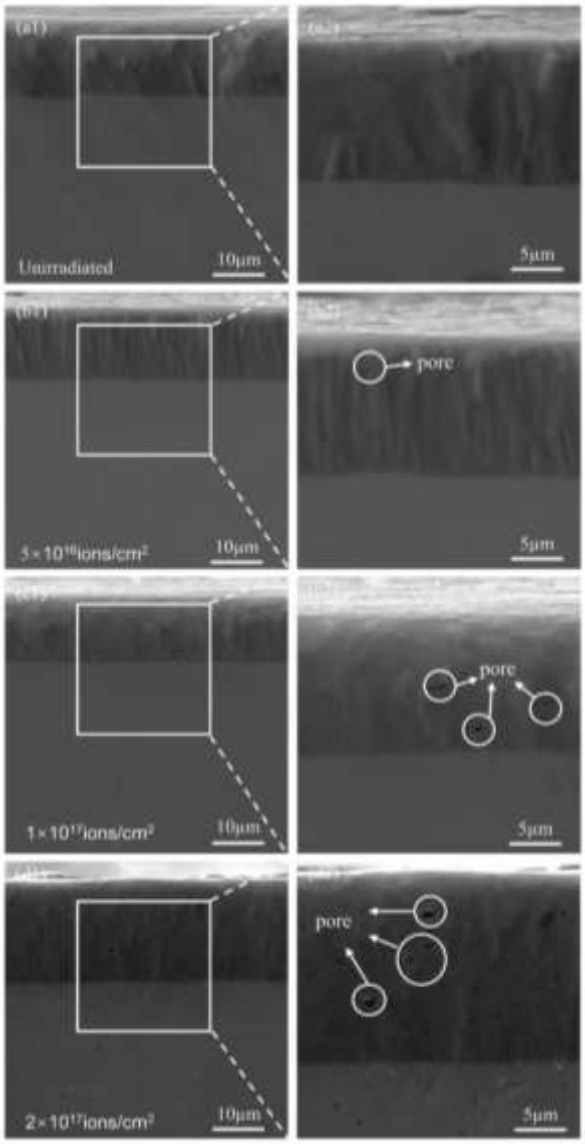

Energy-dispersive spectroscopy (EDS) analysis of the cross-sectional samples, both before and after exposure to varying irradiation doses, revealed that irradiation did not induce significant changes in the elemental composition within the precipitated phase. However, a comparison between the

irradiated and unirradiated samples indicated a notable increase in the concentration of zirconium (Zr) and a corresponding decrease in chromium (Cr) with escalating irradiation doses. This trend is attributed to the formation of irradiation-induced defects, which affect the distribution of these elements within the material.

3.2 Irradiation hardening

Figure 6 indicates the variation in hardness of the coatings with respect to irradiation dose, both before and after irradiation. Overall, the hardness of the irradiated coatings exceeds that of the unirradiated ones.Notably, the hardness reaches a peak of approximately 314.3 HV at an irradiation dose of 5×10^{16} ions/cm^2. Although the hardness value slightly diminishes with further increases in ion fluence, it remains significantly high; for instance, at the highest irradiation dose of 2×10^{17} ions/cm^2, the hardness is still as elevated as 250.9 HV. This suggests that ion irradiation effectively enhances the hardness of the coatings, a phenomenon consistent with the findings of Wang 31, which also reported an increase in hardness following irradiation. The escalation in hardness after irradiation can be attributed to irradiation-induced defects. The accumulation of point defects and defect clusters contributes to an increase in hardness by impeding dislocation slip, a phenomenon referred to as irradiation hardening. This hardening is typically a result of the pinning effect caused by microstructural changes, such as point defect clusters and dislocation loops. While irradiation leads to an increase in the density of dislocation loops, this increase in density leads to a reduction in the material's plastic deformation capacity and a corresponding increase in the hardening effect. The formation of dislocation loops on the surface of the irradiated coatings also accounts for the observed increase in hardness. Furthermore, the hardness tends to decrease as grain refinement on the coating surface intensifies with increasing irradiation dose.

Fig.6. Comparison of hardness between irradiated and unirradiated chromium-coated zirconium alloy sample

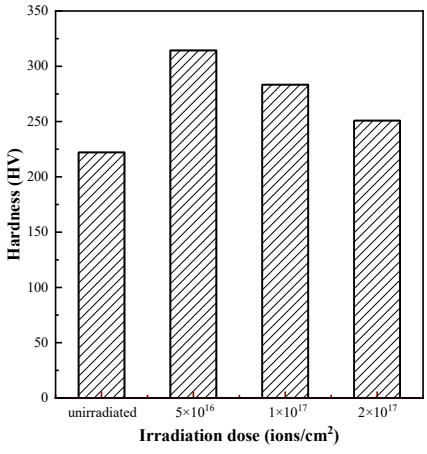

4.Discussion and analysis

The high-energy incident particles during ion irradiation induce a resputtering phenomenon that leads to significant alterations in the large particles on the surface of chromium coatings. This process results in an increase in the number of defects within the cross-section of the chromium coating as the irradiation dose escalates. Concurrently, the depth of ion incidence and the area of defects within the coating also expand. This irradiation-induced defect formation contributes to a pronounced irradiation hardening effect. Although the hardness values exhibit a slight decrease with increasing irradiation

dose, they remain elevated compared to those of the unirradiated samples, indicating the overall enhancement in hardness due to irradiation.

Figure 7 illustrates a comparative TEM cross-sectional analysis of unirradiated chromium coatings and those subjected to an irradiation dose of 2×10^{17}ions/cm^2. The irradiation process induces an increase in the isotropic grain size within chromium coatings. At irradiation doses of 5 and 15 dpa, the average grain size of the coatings remains relatively constant at approximately 250-260 nm. However, at an irradiation dose of 25 dpa, there is a noticeable increase in grain size 32. According to the results of SRIM simulation, the maximum damage can reach 47.4 dpa, and at an irradiation dose of 47.4 dpa, a certain degree of increase in grain size is observed. The average size of columnar crystals in unirradiated chromium coatings is 0.44 μm(Fig.7a2), whereas the average size of columnar crystals in chromium coatings irradiated at a dose of 2×10^{17} ions/cm^2 is 1.31 μm (Fig.7b2) . Grain boundary migration is facilitated by jumps of atoms within the thermal peaks, which are biased by local grain boundary curvature.

The figure demonstrates the alterations microstructure of the chromium coating under irradiation conditions. Initially, the coating contains small dislocation loops, visible as dense black dots in the figure, which are a result of the focused ion beam (FIB) sample preparation (Figure 7 a2). These defect clusters continue to nucleate throughout the irradiation process. As irradiation progresses, multiple dislocation loops form and interact with each other, culminating in the progressive development of a dense dislocation network. With an increasing irradiation dose, there is a noticeable decrease in the number of black dots, and dislocation loops or individual dislocations become more prominent, suggesting that the initial black dots evolve into dislocations (Fig.7b2).

Fig.7. The surface morphology of the unirradiated and irradiated chromium-coated zirconium alloy sample

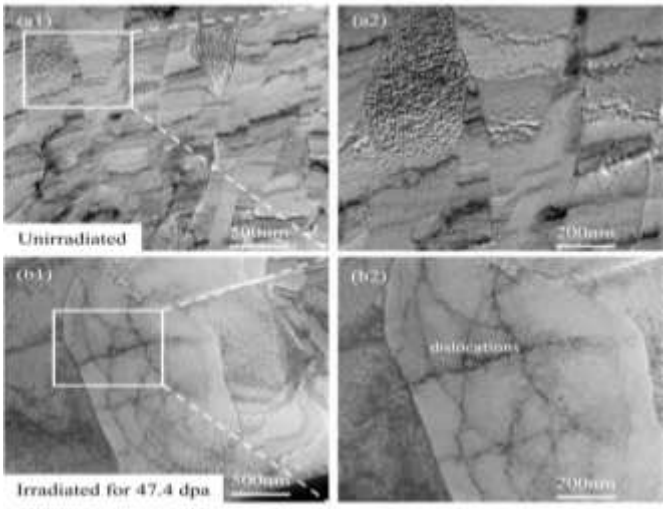

(a) the unirradiated interface (b) the irradiated interface

Figure 8 presents the TEM image of the interface between the zirconium matrix and the chromium coating, both in the unirradiated state and after exposure to an irradiation dose of 2×10^{17} ions/cm^2. The images reveals that there are no dislocations and holes within the zirconium crystal, and no significant structural changes are observed, suggesting that the chromium coating exhibits an excellent resistance to irradiation-induced damage. Furthermore, the absence of pronounced defects at the interface between the zirconium alloy and the chromium coating indicates a strong bond between the two materials.

Fig.8. TEM micrograph of chromium-coated zirconium alloy sample at interface of coating and substrate

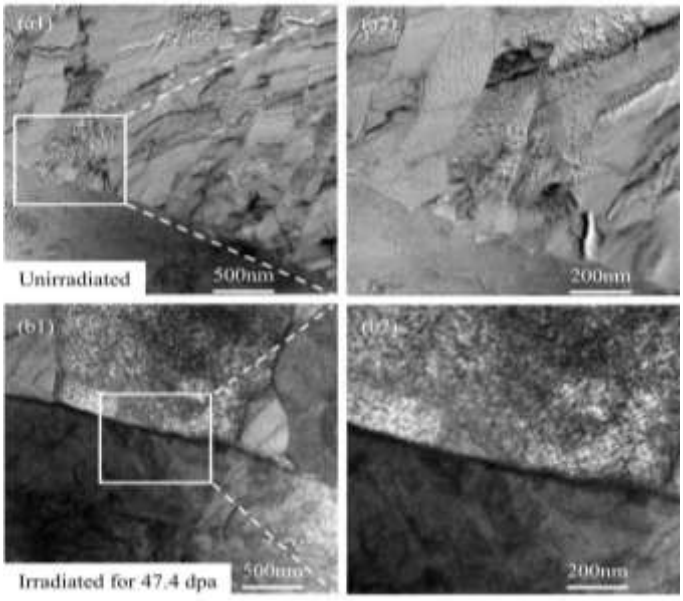

(a) the unirradiated interface (b) the irradiated interface

At an irradiation dose of 47.4 dpa, there is a significant increase in the grain size of the chromium plated layer, which expands from an initial measurement of 0.44 μm to 1.31 μm. During the preparation of the FIB sample, dense black dots, identified as dislocation loops, emerge within the chromium coating. As the irradiation process continues, these dislocation loops multiply and interact, culminating in the progressive development of a dense dislocation network.

5 Conclusion

In the context of nuclear radiation service environment, the radiation dose exerts a profound influence on both the microstructure and mechanical properties of structural materials. This study investigates the impact of Ar^{2+} ion dose on irradiation damage and microstructure evolution of chromium-coated zirconium alloy. Employing a combination of the suite of analytical techniques and SRIM software simulation, the primary conclusions drawn from this research are as follows:

(1) Irradiation did not alter the phase structure of the chromium-coated zirconium alloy. However, the (200) peak broadened post-irradiation and shifted to the right of the standard Cr (200) position. This shift to a higher angle suggests the presence of tensile stress within the material.

(2) High-energy incident particles induced a resputtering phenomenon, leading to significant changes in the large particles on the surface of irradiated chromium-coated zirconium alloy. The number of defects within the chromium-coated zirconium alloy cross-section increased with the irradiation dose, as did the depth of ion incidence and the area of defects.

(3) At an irradiation dose of 47.4 dpa, the grain size of chromium-coated zirconium alloy expanded from 0.44 μm to 1.31 μm. During focused ion beam (FIB) sample preparation, dislocation loops, appearing as dense black dots, were generated in the chromium-coated zirconium alloy. These dislocation loops multiplied and interacted during irradiation, culminating in the formation of a dense

dislocation network.

(4) Irradiation resulted in a pronounced irradiation hardening phenomenon. Although hardness values slightly decreased with increasing irradiation dose, they remained higher than those of unirradiated samples. The chromium-coated zirconium alloy demonstrated good radiation resistance, indicating its potential as a protective material for zirconium alloy fuel cladding in pressurized water reactors.

Acknowledgements

The authors extend their sincere gratitude for the financial support provided by several funding agencies. This research was made possible by the Key Research and Development Program of Hunan Province, under project number 2022SK2095. Additional support was received from the Natural Science Foundation of Hunan Province, with the project number 2023JJ50130. The Hengyang Science and Technology Planning Project also contributed to this work, with the project number 202150084056. The contributions of these organizations are greatly appreciated and have been instrumental in the successful execution of this research.

References

1. Terrani, K. A. (2018). Accident tolerant fuel cladding development: Promise, status, and challenges. Journal of Nuclear Materials, 501, 13-30.
2. Alabdullah, M., & Ghoniem, N. M. (2020). A thermodynamics-based damage model for the non-linear mechanical behavior of SiC/SiC ceramic matrix composites in irradiation and thermal environments. International Journal of Damage Mechanics, 29(10), 1569-1599.
3. Deck C P, Jacobsen G M, Sheeder J, et al. Characterization of SiC–SiC composites for accident tolerant fuel cladding[J]. Journal of Nuclear Materials, 2015, 466: 667-681.
4. Yamamoto, Y., Pint, B. A., Terrani, K. A., Field, K. G., Yang, Y., & Snead, L. L. (2015). Development and property evaluation of nuclear grade wrought FeCrAl fuel cladding for light water reactors. Journal of Nuclear Materials, 467, 703-716.
5. Kim, H. G., Kim, I. H., Jung, Y. I., Park, D. J., Park, J. Y., & Koo, Y. H. (2015). Adhesion property and high-temperature oxidation behavior of Cr-coated Zircaloy-4 cladding tube prepared by 3D laser coating. Journal of Nuclear Materials, 465, 531-539.
6. Shah, H., Romero, J., Xu, P., Maier, B., Johnson, G., Walters, J., ... & Sridharan, K. (2017). Development of surface coatings for enhanced accident tolerant fuel. Water React. Fuel Perform. Meet., Jeju Island, Korea.
7. Tang, C., Stueber, M., Seifert, H. J., & Steinbrueck, M. (2017). Protective coatings on zirconium-based alloys as accident-tolerant fuel (ATF) claddings. Corrosion reviews, 35(3), 141-165.
8. Alat, E., Motta, A. T., Comstock, R. J., Partezana, J. M., & Wolfe, D. E. (2016). Multilayer (TiN, TiAlN) ceramic coatings for nuclear fuel cladding. Journal of Nuclear Materials, 478, 236-244.
9. Yazhen, W., Hang, X., Guoyun, L., **aosong, L., Haisheng, Z., Kai, S., ... & Shasha, L. (2023). Influence of Neutron Irradiation on Mechanical Properties of Cr-coated Zirconium Alloy. Nuclear Power Engineering, 44(2), 116-121.
10. Huang, H., Changjun, Q., Chen, Y., Liangbin, H., Yanhong, L., & Huailin, **. (2018). High temperature oxidation resistance of magnetron sputtering and multi-arc ion plating Cr films on zirconium alloy. China Surface Engineering, 31(2), 51-58.
11. Yang, H. Y., Zhang, R. Q., Peng, X. M., & Wang, M. L. (2017). Research progress regarding

surface coating of zirconium alloy cladding. Surf. Technol, 46(1), 69-75.
12. Kuprin, A. S., Belous, V. A., Voyevodin, V. N., Bryk, V. V., Vasilenko, R. L., Ovcharenko, V. D., ... & V'yugov, P. N. (2015). Vacuum-arc chromium-based coatings for protection of zirconium alloys from the high-temperature oxidation in air. Journal of Nuclear Materials, 465, 400-406.
13. Yang, Z., Cheng, Z., Qiu, J., Wu, Z., Zhang, H., & Ran, G. (2017). Study on corrosion resistance of Zr-0.8 Sn-1Nb-0.3 Fe alloy after Kr^+ ion irradiation. Nuclear Power Engineering, 38(5), 123-128.
14. Huang, M., Li, Y., Ran, G., Yang, Z., & Wang, P. (2020). Cr-coated Zr-4 alloy prepared by electroplating and its in situ He^+ irradiation behavior. Journal of Nuclear Materials, 538, 152240.
15. Li, Y., Li, Y., & **ao, W. (2019). Point defects and grain boundary effects on tensile strength of 3C-SiC studied by molecular dynamics simulations. Nuclear Engineering and Technology, 51(3), 769-775.
16. Gabriel, A., Hawkins, L., French, A., Li, Y., Hu, Z., He, L., ... & Shao, L. (2022). Effect of dpa rate on the temperature regime of void swelling in ion-irradiated pure chromium. Journal of Nuclear Materials, 561, 153519.
17. Kim, H., Ryabikovskaya, E., French, A., Gabriel, A., Wang, T., Shirvan, K., ... & Shao, L. (2020). Irradiation-induced swelling of pure chromium with 5 MeV Fe ions in the temperature range 450–650° C. Journal of Nuclear Materials, 543(LA-UR-20-22579).
18. Yoon, S. Y., Lee, K. O., Kang, S. S., & Kim, K. H. (2002). Comparison for mechanical properties between TiN and TiAlN coating layers by AIP technique. Journal of materials processing technology, 130, 260-265.
19. Stoller, R. E., Toloczko, M. B., Was, G. S., Certain, A. G., Dwaraknath, S., & Garner, F. A. (2013). On the use of SRIM for computing radiation damage exposure. Nuclear instruments and methods in physics research section B: beam interactions with materials and atoms, 310, 75-80.
20. Nastasi, M., Mayer, J. W., & Hirvonen, J. K. (1996). Ion-solid interactions: fundamentals and applications. Cambridge University Press.
21. Ziegler, J. F., & Biersack, J. P. (1985). The stop** and range of ions in matter. In Treatise on heavy-ion science: volume 6: astrophysics, chemistry, and condensed matter (pp. 93-129). Boston, MA: Springer US.
22. Egeland, G. W., Valdez, J. A., Maloy, S. A., McClellan, K. J., Sickafus, K. E., & Bond, G. M. (2013). Heavy-ion irradiation defect accumulation in ZrN characterized by TEM, GIXRD, nanoindentation, and helium desorption. Journal of nuclear materials, 435(1-3), 77-87.
23. Egeland, G. W., Valdez, J. A., Maloy, S. A., McClellan, K. J., Sickafus, K. E., & Bond, G. M. (2013). Heavy-ion irradiation defect accumulation in ZrN characterized by TEM, GIXRD, nanoindentation, and helium desorption. Journal of nuclear materials, 435(1-3), 77-87.
24. Wan, H., Si, N., Chen, K., & Wang, Q. (2015). Strain and structure order variation of pure aluminum due to helium irradiation. RSC advances, 5(92), 75390-75394.
25. Lin, J. C., Hoffman, R. A., & Panseri, N. J. (1997). Effect of ion bombardment on the structure and properties of polycrystalline chromium films. MATERIAL AND MANUFACTURING PROCESS, 12(2), 329-343.
26. Thornton, J. A., & Hoffman, D. W. (1989). Stress-related effects in thin films. Thin solid films, 171(1), 5-31.
27. Doerner, M. F., & Nix, W. D. (1988). Stresses and deformation processes in thin films on substrates. Critical Reviews in Solid State and Material Sciences, 14(3), 225-268.
28. Shiao, M. H., & Shieu, F. S. (2001). A formation mechanism for the macroparticles in arc

ion-plated TiN films. Thin solid films, 386(1), 27-31.
29. Wang, H., Qiu, C., Zeng, X., Zhang, W., Wang, X., Liu, Y., & Li, H. (2017). Effect of Temperature on Morphology and Corrosion Resistance of Pure Cr Coating. Surf. Technol, 46, 192-196.
30. Yang, T. N., Lu, C., **, K., Crespillo, M. L., Zhang, Y., Bei, H., & Wang, L. (2017). The effect of injected interstitials on void formation in self-ion irradiated nickel containing concentrated solid solution alloys. Journal of Nuclear Materials, 488, 328-337.
31. Wang, R., Li, B., Li, P., Bai, X., Hu, L., Huang, Q., ... & Ge, F. (2021). Effect of low-dose Xe20+ ion irradiation on the deformation behavior of the magnetron sputtered coatings under nanoindentation. Surface and Coatings Technology, 428, 127907.
32. Kuprin, A. S., Belous, V. A., Voyevodin, V. N., Vasilenko, R. L., Ovcharenko, V. D., Tolstolutskaya, G. D., ... & Kolodiy, I. V. (2018). Irradiation resistance of vacuum arc chromium coatings for zirconium alloy fuel claddings. Journal of Nuclear Materials, 510, 163-167.